Layer-spinel heterostructure $0.5NaMnO_2$-$0.5Li_{0.5}Mn_2O_4$ cathode for high performance lithium ion batteries

Tianfeng Gao,[a,b] Yanjun Cai,[a,b,*] Qingrong Kong,[a,b] Hualing Tian,[a,b] Xiang Yao,[a,b] Zhi Su[a,b,c,*]

[a] College of Chemistry and Chemical Engineering, Xinjiang Normal University, Urumqi, 830054, Xinjiang, China

[b] Xinjiang Key Laboratory of Energy Storage and Photoelectrocatalytic Materials, Urumqi, 830054, Xinjiang, China

[c] Xinjiang Institute of Technology, China

* Corresponding author. College of Chemistry and Chemical Engineering, Xinjiang Normal University, Urumqi, 830054, Xinjiang, China.

E-mail address: cyjxjsf@yeah.net，suzhixj@sina.com (Z. Su).

The heterojunction cathode materials $NaMnO_2$-$Li_{0.5}Mn_2O_4$ were synthesized by solid-phase method. Using Na_2CO_3, $LiOH•H_2O$ and MnO_2 as raw materials with the molar ratio of Na:Li:Mn = X:0.2:0.8 (X=0.2, 0.4, 0.6 and 0.8). with increasing the content of sodium, the content of $NaMnO_2$ increasing from weight 49.74% to 69.30% in the NLMO-2 and NLMO-3, respectively. The Na-Li-Mn ratio is the most critical factor that determines the phase of Na_xMnO_2 products.[1] When the molar ratio of Na:Li:Mn = 0.8:0.2:0.8, the $Na_{0.66}MnO_2$ (space group: P63/mmc) and $NaMnO_2$ (space group: Cmcm) was formed, corresponding proportion was 81.36%:18.64%. This phenomenon is attributed to the lithium may doped into $Na_{0.66}MnO_2$ and $NaMnO_2$, and the phase of $Na_{0.66}MnO_2$ preferential formation.

Table S1 Rietveld analysis of as-prepared samples

samples	Chemical Formula (Ratio)
NLMO-1	$LiMn_2O_4$
NLMO-2	$Li_{0.5}Mn_2O_4$ (50.26%), $NaMnO_2$ (49.74%)
NLMO-3	$Li_{0.5}Mn_2O_4$ (30.70%), $NaMnO_2$ (69.30%)
NLMO-4	$Na_{0.66}MnO_2$ (81.36%), $NaMnO_2$ (18.64%)

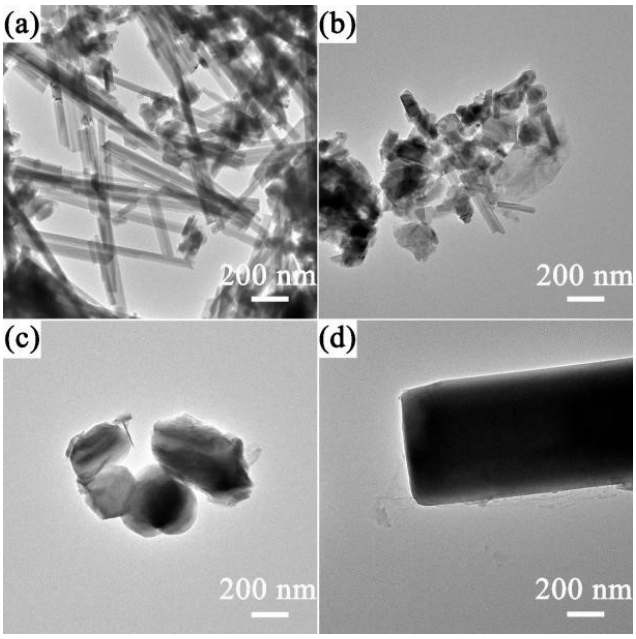

Fig. S1. TEM image of NLMO sample (a) NLMO-1, (b) NLMO-2, (c) NLMO-3, (d) NLMO-4.

The initial charge/discharge was 136.1/118.5 mA h g^{-1}, after 500 cycles it was maintain at 110.2/104.1 mA h g^{-1}, at current of 500 mA g^{-1}, as shown in Fig. S2.

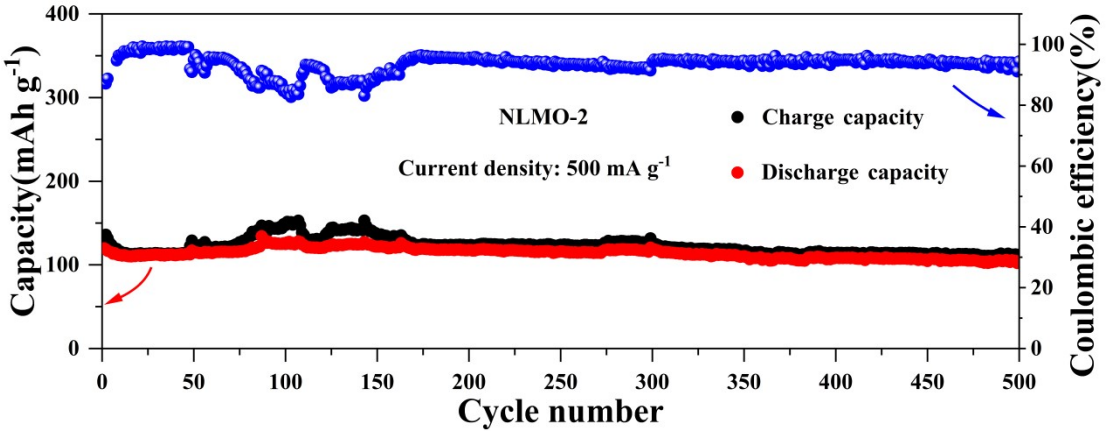

Fig. S2 The long-term cycle stability of NLMO-2 at current density of 500 mA g^{-1} for LIBs.

The XRD patterns of NLMO-2 before cycling and after1000 cycles at 2 A g^{-1}, as displayed in Fig. S3. The main structure of NLMO-2 remains unchanged at high current density of 2 A g^{-1} and long terms cycle, which showing ultra-high structural reversibility.

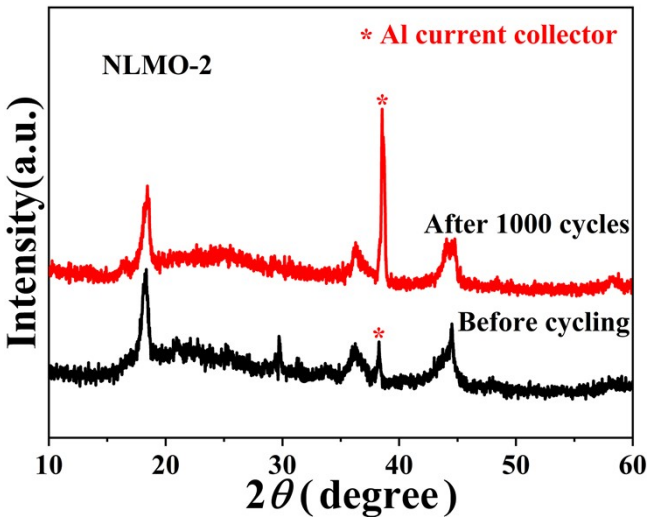

Fig. S3 The XRD patterns of NLMO-2 before cycle and after 1000 cycles at current density of 2 A g^{-1} for LIBs.

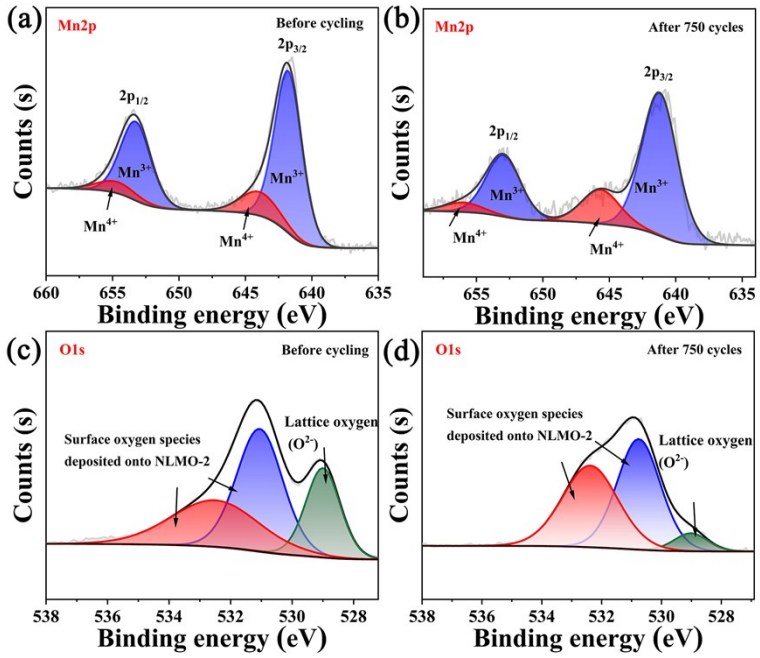

Fig. S4 The O1s and Mn2p XPS spectra of NMLO-2 before cycle and after 750 cycles for LIBs.

XPS was utilized to investigate the binding state of manganese and oxygen in $NaMnO_2$-$Li_{0.5}Mn_2O_4$, as illustrated in Fig. S4. The Mn^{3+} peak areas of NLMO-2 before cycle in Fig. S4(a) were observed at 641.77 eV and 653.26 eV, with contents of 54.23% and 29.56%, corresponding to Mn^{3+} 2p3/2 and Mn^{3+} 2p1/2, respectively. The Mn^{4+} peaks of NLMO-2 before cycle were found at 643.98 eV and 654.77 eV, with contents of 11.00% and 5.21%, corresponding to Mn^{4+} 2p3/2 and Mn^{4+} 2p1/2, respectively. After 750 cycles at 1 A g^{-1}, the Mn^{3+} peak areas of NLMO-2 in Fig. S4(b) were observed at 641.22 eV and 652.97 eV, with contents of 56.97% and 24.23%, corresponding to Mn^{3+} 2p3/2 and Mn^{3+} 2p1/2, respectively. The Mn^{4+} peaks of NLMO-2 were found at 645.66 eV and 656.00 eV, with contents of 14.72% and 4.08%, corresponding to Mn^{4+} 2p3/2 and Mn^{4+} 2p1/2, respectively.

The O1s peak areas of NLMO-2 (before cycle) are depicted in Fig. S4(c). The peaks at 529.00 eV, and 531.05 eV, 532.50 eV correspond to lattice oxygen (O^{2-}) and surface-deposited oxygen, with a content of 23.97% and 76.03%, respectively. After 750 cycles at 1 A g^{-1}, the O1s peak areas of NLMO-2 are depicted in Fig. S4(d). The peaks at 529.02 eV and 530.76 eV, 532.38 eV correspond to lattice oxygen (O^{2-}), and surface-deposited oxygen, with a content of 6.08% and 93.92%, respectively. Compared to the pristine NLMO-2 (before cycle), the surface-deposited oxygen was increased at high current density of 1 A g^{-1} after 750 cycles. However, it still exhibit an excellent cycle stability as shown in Fig.4d. The initial charge/discharge was 172.6/107.1 mA h g^{-1}, after 750 cycles it keeps 105.6/88.1 mA h g^{-1}, at current of 1 A g^{-1}.

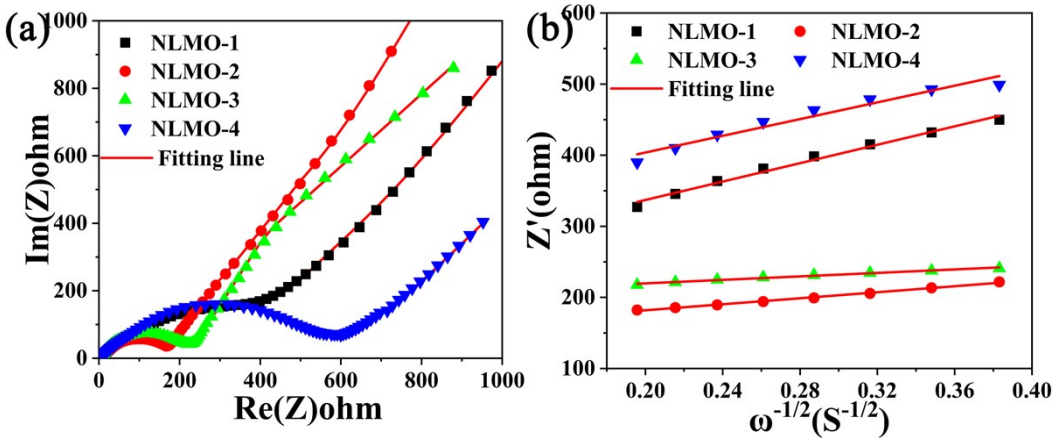

Fig. S5. The EIS of NLMO in LIBs (a) the AC impedance, (b) the equivalent circuit fitting curve.

Table S2 Data of each electrochemical component of as-prepared samples.

samples	R_1 (Ω)	R_2 (Ω)	D_{Li}^+(cm^2 s^{-1})
NLMO-1	0.36	656.4	1.37×10^{-10}
NLMO-2	3.68	167.0	1.28×10^{-9}
NLMO-3	4.35	225.0	3.83×10^{-9}
NLMO-4	3.88	607.9	1.66×10^{-10}

R_1: solution impedance, R_2: charge transfer impedance.

In order to further explore the conductivity of prepared samples, the electrochemical impedance were tested, respectively, as shown in Fig. S5. The AC impedance diagram is mainly composed of three parts. The intersection of the semi-circle and the real axis in AC impedance is the total internal resistance (Rs). The fitting data are shown in Table 1. In the AC impedance test of LIBs, the resistance of NLMO-2 (167.0 Ω) is much smaller than that of NLMO-3(255.0 Ω), NLMO-1(656.4 Ω) and NLMO-4(607.9 Ω). The lowest charge transfer resistance is beneficial to improve the charge transfer rate, so NLMO-2 shows well rate performance. In addition, the diagonal line of Li^+ ions migration rate of NLMO-2 is closer to the X-axis, indicating that the $0.5NaMnO_2$-$0.5Li_{0.5}Mn_2O_4$ has a higher Li^+ ions migration rate than the others.

The dynamics of heterostructures cathodes were studied, the lithium diffusion coefficients (D_{Li}^+) were calculated through the equation (1) and equation (2)

$$Z=R_1+R_2+\delta\omega^{-1/2} \quad (1)$$

$$D=R^2T^2/2n^4\delta^2C^2A^2F^4 \quad (2)$$

Where R is the gas constant (8.3145 J mol^{-1} K^{-1}), T is the thermodynamic temperature (298 K), C is the concentration of Li^+, n is the electron transfer number, A is the electrode surface area (0.785 cm^2), and F is the Faraday constant (96485 C mol^{-1}). As shown in Table S2, the D_{Li}^+ values for NLMO-1 to NLMO-4 were 1.37×10^{-10}, 1.28×10^{-9}, 3.83×10^{-9}, 1.66×10^{-10} cm^2 s^{-1}. The D_{Li}^+ of NLMO-2

and NLMO-3 were larger than those of NLMO-1 and NLMO-4. These results indicate that the $0.5NaMnO_2$-$0.5Li_{0.5}Mn_2O_4$ heterostructure can effectively accelerate the electrochemical reaction kinetics of Li^+ ions intercalation and deintercalation.

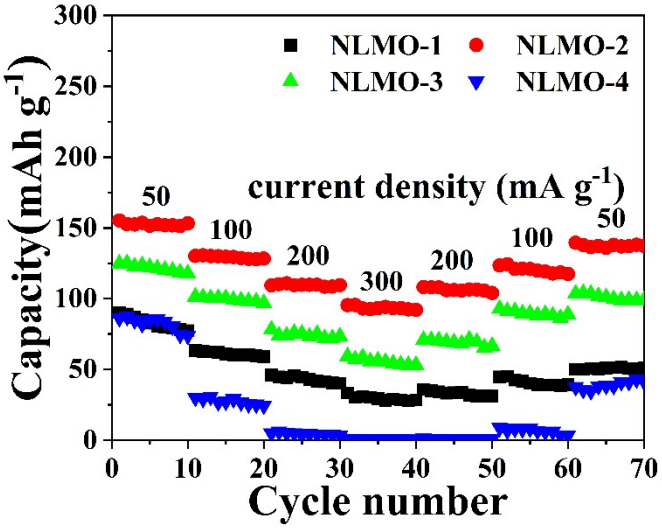

Fig. S6. The rate performance of as-prepared samples of the heterostructure NLMO in SIBs.

Fig. S6 is rate performance of NLMO for SIBs, which was activated at current density of 10 mA g^{-1} for 10 cycles. The rate performances tested at current densities of 50 mA g^{-1} to 300 mA g^{-1}. The NLMO-1 rate discharge capacities were 90.2, 63.4, 46.2 and 33.4 mA h g^{-1} at current densities of 50, 100, 200 and 300 mA g^{-1}; 155.2, 130.2, 109.4 and 95.4 mA h g^{-1} for NLMO-2; 124.8, 101.3, 78.1 and 59.2 mA h g^{-1} for NLMO-3; 86.3, 30.2, 5 and 0.9 mA h g^{-1} for NLMO-4. With the rate current densities back to 200, 100 and 50 mA g^{-1}, the discharge capacities of NLMO-1 were 35.9, 44.7, and 50.2 mA h g^{-1}; 108.2, 123.5 and 139.5 mA h g^{-1} for NLMO-2; 70.8, 92.8 and 103.5 mA h g^{-1} for NLMO-3; 1.3, 8.8 and 37.7 mA h g^{-1} for NLMO-4. Compared to NLMO-1, NLMO-3, and NLMO-4, the NLMO-2 shows the best rate performance when sodium content X=0.4.

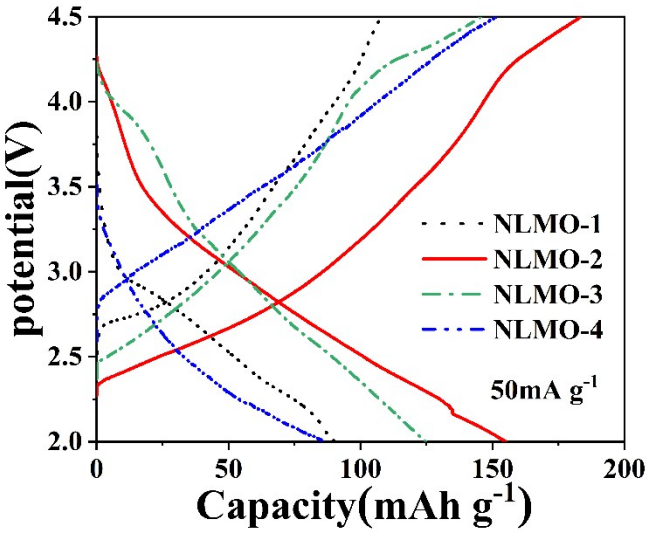

Fig. S7. The initial charge-discharge curves of as-prepared samples of the heterostructure NLMO in SIBs .

Fig. S7 is initial charge-discharge curves of NLMO in SIBs, which was activated for 10 cycles at current density of 10 mA g^{-1} and tested at the current density of 50 mA g^{-1}. During the charging and discharging process, NLMO-1 observed a pair of voltage plateaus around 2.5 V. From the NLMO-2, it can be observed a smoother voltage plateau than NLMO-1 at about 2.5 V. With the increase of sodium content in the material, a pair of voltage plateaus were observed at about 4 V, it is speculated that the appearance of this plateau is related to triggering anionic oxygen redox. A pair of voltage plateaus around 3.3 V was observed from NLMO-3, and the same voltage plateaus as NLMO-2 were observed around 4 V, and the plateaus were longer. A pair of voltage plateaus around 2.3 V and a pair of voltage plateaus around 4 V was observed from NLMO-4. The voltage plateaus alter demonstrated that spinel phase was existing in NLMO-1, NLMO-2, NLMO-3 and disappear in NLMO-4, which agree well with the analysis of XRD.

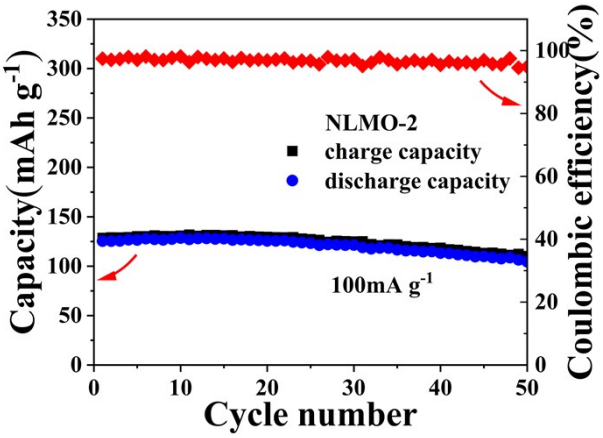

Fig. S8. Cycle performance of the as-prepared samples of the heterostructure NLMO in SIBs

Fig. S8 show cycle performance of NLMO for SIBs at current density of 100 mA g^{-1}. The initial charge/discharge capacity of NLMO-2 was128.64/125.34 mA h g^{-1} at 100 mA g^{-1}. After 50 cycles, the charge/discharge capacity was maintained at 107.96/103.79 mA h g^{-1}, the capacity retention rate reached 83.92%/82.81%, and the coulombic efficiency keep 96.14%. The cycle performance of the material shows obvious fading, which is attributed to the irreversible anion oxidation-reduction at high voltage, especially when the voltage is higher than 4.0 V.

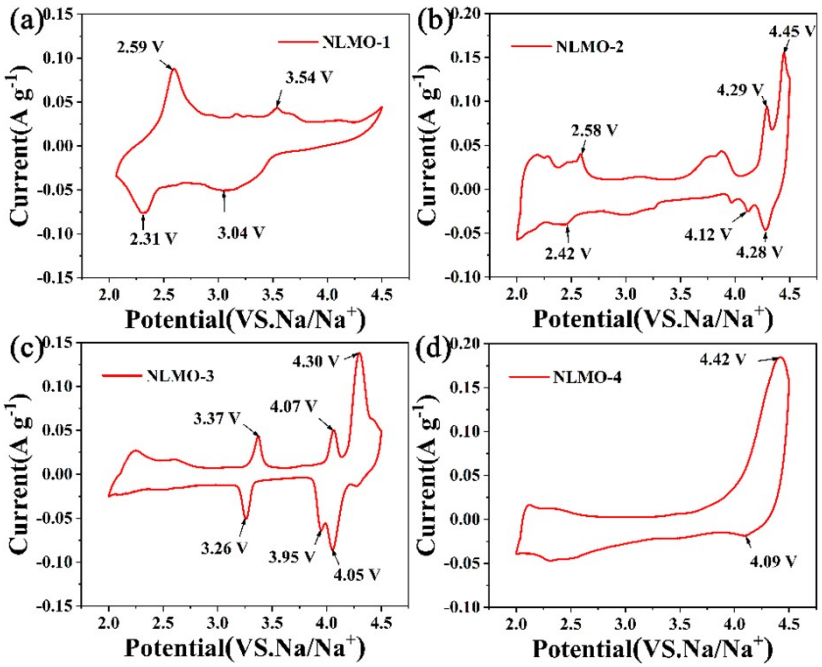

Fig. S9. CV curves of NLMO for SIBs. (a) NLMO-1；(b) NLMO-2；(c) NLMO-3；(d) NLMO-4.

In order to further explore the influence of Na content on heterostructure NLMO cathode materials, the CV test was carried out on the as-prepared samples within the voltage range of 2-4.5 V at scanning rate of 0.1 mV s^{-1}. The CV curves is shown in Fig. S9. Two pairs of redox peaks of NLMO-1 are located at 2.59 V, 3.54 V and 2.31 V, 3.04 V. The three redox peaks of NLMO-2 are located at 2.42 V, 4.12 V, 4.28 V and 2.58 V, 4.29 V, 4.45 V. The three redox peaks of NLMO-3 are located at 3.26 V, 3.95 V, 4.05 V and 3.37 V, 4.07 V, 4.30 V. The two redox peaks of NLMO-4 are located at 4.09 V and 4.42 V.

The redox peak of 2.3-2.6 V in NLMO-1, NLMO-2, and NLMO-3 corresponds to Na^+ is insert into the spinel $LiMn_2O_4/Li_{0.5}Mn_2O_4$ and forms $Na_xLiMn_2O_4/Na_xLi_{0.5}Mn_2O_4$. During charging, Na^+ is remove from $Na_xLiMn_2O_4/Na_xLi_{0.5}Mn_2O_4$ to form $LiMn_2O_4/Li_{0.5}Mn_2O_4$.[2] The electrochemical reaction is as follows equation (3):

$$LiMn_2O_4/Li_{0.5}Mn_2O_4 + xNa^+ + xe^- \leftrightarrow Na_xLiMn_2O_4/Na_xLi_{0.5}Mn_2O_4 \quad (3)$$

With the increasing of Na content, the proportion of $Li_{0.5}Mn_2O_4$ in NLMO material decreases gradually, and some parts form a heterostructure. Therefore, the intensity of oxidation-reduction peaks decreases gradually at 2.3-2.6 V. The redox peak of 3.0-3.5 V corresponds to Na^+ is extracted from layered $NaMnO_2$ and forms $Na_{1-x}MnO_2$, resulting in the formation of vacancies in the electrode material.[3] During the discharge, Na^+ is inserted into the vacancy, and the electrochemical reaction is as follows equation (4):

$$NaMnO_2 \leftrightarrow Na_{1-x}MnO_2 + xNa^+ + xe^- \quad (4)$$

The oxidation-reduction peaks located at 3.9-4.5 V was generated from the oxidation-reduction of the anionic oxygen, and O^{2-} in the material was oxidized into products such as molecular O_2, peroxide and superoxide $(O_2)^{n-}(n<2)$ in the organic phase.[4] However, the oxidation-reduction peaks of NLMO-4 is significantly different from that of NLMO-2 and NLMO-3. The reason can be attributed to the irreversible structural transformation and structural collapse in the material due to the excessive Na content.

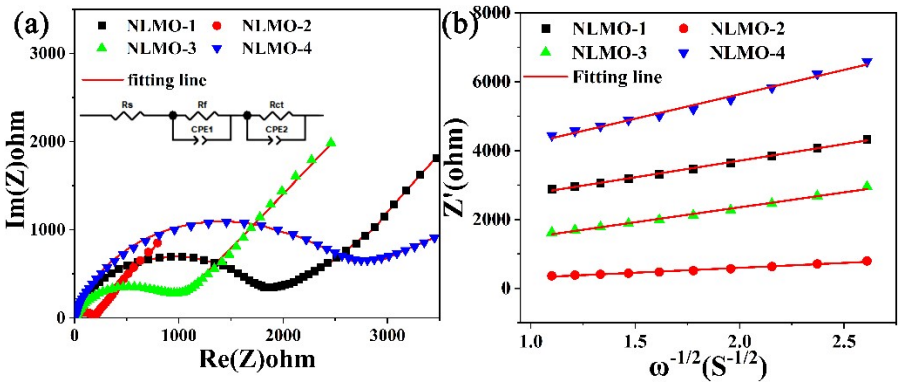

Fig. S10. The samples of NLMO for SIBs (a) the AC impedance. (b) the equivalent circuit fitting curve.

Table S3 Data of electrochemical components of as-prepared samples.

samples	R_s (Ω)	R_f (Ω)	D_{Na^+}(cm^2 s^{-1})
NLMO-1	4.41	1835.00	8.21×10^{-14}
NLMO-2	8.55	180.10	9.47×10^{-13}
NLMO-3	5.72	977.30	1.01×10^{-13}
NLMO-4	4.70	2776.00	3.80×10^{-14}

R_s: solution impedance, R_f: charge transfer impedance.

The fitting data are shown in and Table S3. The resistance of NLMO-2 (180.10 Ω) is much smaller than that of NLMO-3 (977.30 Ω), NLMO-1 (1835.00 Ω), and NLMO-4 (2776.00 Ω) in that AC impedance testing of SIBs. The lowest charge transfer resistance is advantageous to increase the charge transfer rate, so that NLMO-2 shows a good rate performance. In addition, the diagonal line of ion migration rate of NLMO-2 is closer to the X axis, indicating that the sample has a higher sodium ion migration rate. The D_{Na^+} values for NLMO-1 to NLMO-4 were 8.21×10^{-14}, 9.47×10^{-13}, 1.01×10^{-13} and 3.80×10^{-14} cm^2 s^{-1}, respectively. The D_{Na^+} of NLMO-2 were greater than those of NLMO-1, NLMO-3 and NLMO-4. These results indicate that the $NaMnO_2$-$Li_{0.5}Mn_2O_4$ heterostructure can effectively accelerate the electrochemical reaction kinetics of Na^+ intercalation and deintercalation.

Based on the stable cyclability and reversible structure evolution of NLMO-2 in the half cell, a hard carbon assembled full cell was tested in the range of 2.0-4.5 V. The capacity of cathode and anode was in the range of 1:1.2 to guarantee sufficient (de) insertion sites for Li^+ ions. As revealed in Fig. S11, the full-cell device exhibited well

cycle performance, the initial charge/discharge was 197.3/174.1 mA h g^{-1}, after 30 cycles it maintains at 168.7/141.9 mA h g^{-1} with mass loading of 1.36 mg cm^{-2} at current density of 100 mA g^{-1}. The NLMO-2//hard carbon full cell exhibited a high energy density of≈484.00 Wh kg^{-1} with an average operation voltage of 2.78 V.

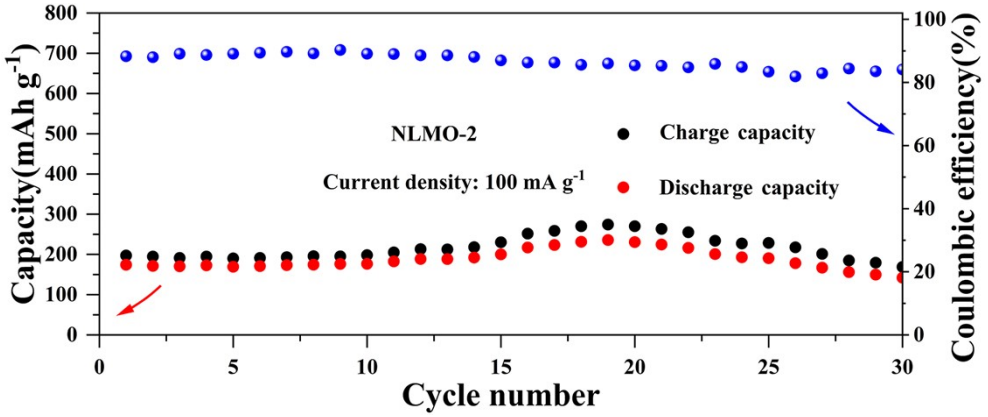

Fig. S11 Electrochemical performance of NLMO-2//hard carbon in the voltage range of 2.0-4.5 V for lithium batteries.

To confirm the suitability of the present $NaMnO_2$ as a cathode for SIBs, we fabricated full cells paired with hard carbon anodes after adjusting the N/P capacity ratio of 1.2 (Fig. S12). The initial charge/discharge was 90.5/83.2 mA h g^{-1}, after 10 cycles it was 73.7/69.2 mA h g^{-1} with mass loading of 3.84 mg cm^{-2} at current density

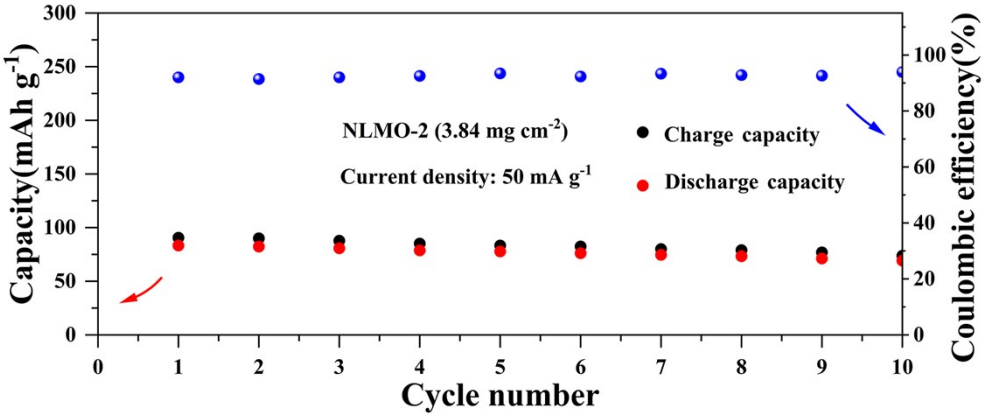

Fig. S12 Electrochemical performance of NLMO-2//hard carbon in the voltage range of 2.0-4.5 V for sodium batteries.

of 50 mA g^{-1}. The NLMO-2//hard carbon full cell exhibited a high energy density of ≈223.81 Wh kg^{-1} with an average operation voltage of 2.69 V.

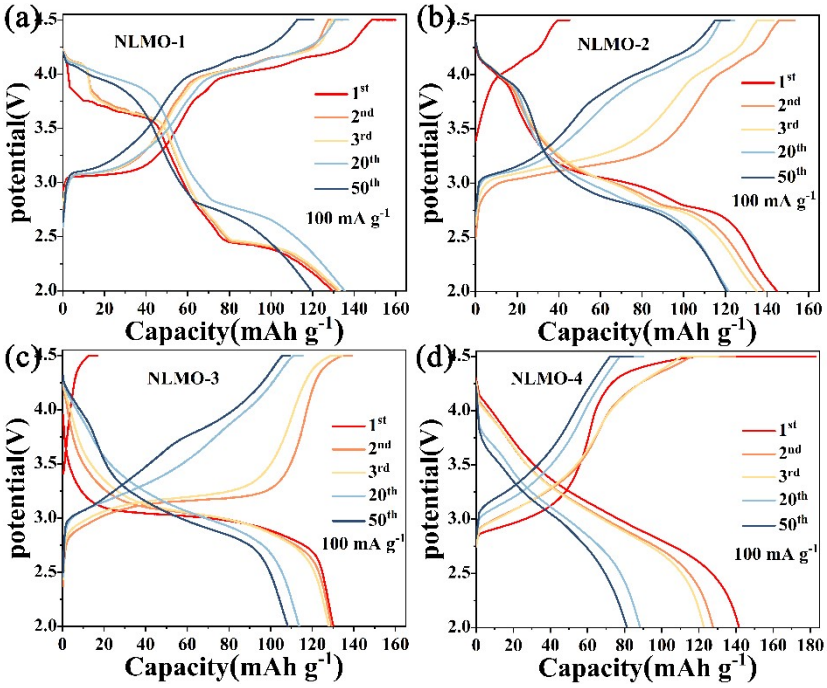

Fig. S13. The charge-discharge curves of as-prepared samples of the heterostructure NLMO in LIBs (a) NLMO-1, (b) NLMO-2, (c) NLMO-3, (d) NLMO-4.

Notes and references

1. W.H. Zuo, Y. Yang, *Acc. Mater. Res.*, 2022, **3**, 709-720.

2. R. A. House, G. J. Rees, M. A. Pérez-Osorio, J.-J. Marie, E. Boivin, A. W. Robertson, A. Nag, M. Garcia-Fernandez, K.-J. Zhou and P. G. Bruce, *Nature Energy*, 2020, **5**, 777-785.

3. Y. Yu, D. Ning, Q. Li, A. Franz, L. Zheng, N. Zhang, G. Ren, G. Schumacher and X. Liu, *Energy Storage Materials*, 2021, **38**, 130-140.

4. C. Zhao, C. Li, H. Liu, Q. Qiu, F. Geng, M. Shen, W. Tong, J. Li and B. Hu, *J. Am. Chem. Soc.*, 2021, **143**, 18652-18664.